Catalysis Letters Vol. 111, Nos. 3–4, November 2006 (© 2006)
DOI: 10.1007/s10562-006-0150-7

SAPO-11/HBeta composites for catalytic cracking of 2-butylene: effects of defect structure

Xin Zhang,[a,b,*] Jianwei Wang,[a] Jin Zhong,[a] Aisong Liu,[a] and Junkui Gao[a]

[a]*Research Institute of Petroleum Processing, Xue Yuan Road 18, P.O. Box 914-4, Beijing, 100083, P.R. China*
[b]*Institute fur Experimtalphysik, Fachbereich Physik, Freie Universitat Berlin, Arnimallee 14, Berlin, D-14195, Germany*

Received 14 July 2006; accepted 20 July 2006

SAPO-11/HBeta composite was synthesized by using hydrothermal method (SB-H) and applied as catalyst for cracking of 2-butylene to C_2–C_3 olefins. SB-H sample exhibited comparatively high selectivity and high yield of C_2–C_3 olefins. XRD, IR, ^{27}Al and ^{31}P MAS NMR, Py-IR characterizations indicate that defect structure $P(AlO_4)_n$ ($n < 4$) really existed in SB-H sample. SAPO-11 and HBeta chemically bonded and the defect $P(AlO_4)_n$ ($n < 4$) formed during the hydrothermal synthesis of SB-H sample. $P(AlO_4)_n$ ($n < 4$) unit caused new B acidic sites, which increased B acidic amount and B acidic distribution on SB-H sample. The improvement of B acidity decreased apparent active energy of cracking of 2-butylene to C_2–C_3 olefins on SB-H sample. Therefore, the high selectivity and high yield of C_2–C_3 olefins were obtained on SB-H sample in catalytic cracking of 2-butylene.

KEY WORDS: SAPO-11; HBeta; composite molecular sieve; defect structure; butylene; catalytic cracking; acidic property.

1. Introduction

Catalytic cracking of C_4 olefin to propylene and ethylene has attracted much attention because it is an alternative route to produce valuable chemical from cheap resource whether by using fixed bed reactor or FCC reactor system [1–6]. Up to date, a few zeolite-based catalysts have been developed. Lu *et al.* [2] reported that 12.63%wt selectivity of propylene at 83.50%wt conversion of 1-butylene was obtained on CC-16 + 5%wt RPSA zeolite catalyst at 500 °C and WHSV = 4.92 h^{-1}. Wang *et al.* [3] found that the as-synthesized ZSM-23 (SiO_2/Al_2O_3 = 30) showed 32.9% yield of propylene and 19.28% yield of ethylene at ca. 80% conversion of 2-butylene at 873 K and WHSV = 2.5 h^{-1}. Zhu *et al.* [4,5] considered that among ZSM-5, ZSM-22, ZSM-23, ZSM-35, SAPO-34 and MCM-22, the smaller the pore size of the molecular sieve was, the higher the initial selectivity of C_2–C_3 olefins. In order to obtain high selectivity and yield of C_2–C_3 olefins in catalytic cracking of C_4 olefin, it is necessary to develop new catalytic material and deeply understand its structure–function relation.

In this present work, novel SAPO-11/HBeta composite was synthesized by hydrothermal method (SB-H). Binary structure composite molecular sieve not only combines the advantages of the two distinct kinds of molecular sieve, but also induces special properties which can affect catalytic performance. We comparatively investigated physicochemical properties and catalytic performance of SB-H sample in cracking of 2-butylene by S_{BET}, XRD, IR, ^{27}Al and ^{31}P MAS NMR and catalytic test technologies. Defect structure in SB-H sample was observed. The effects of the defect structure on the properties and catalytic performance are discussed.

*To whom correspondence should be addressed.
E-mail: zhangxinzhangcn@yahoo.com.cn

2. Experimental

2.1. Synthesis

2.1.1. Hydrothermal synthesis method

SAPO-11/HBeta composite was synthesized with hydrothermal method. The sample was denoted as SB-H. A typical synthesis procedure was as following: (1) 11.97 g of H_3PO_4 (85 wt%, Beijing Chem. Co., AR), 5.58 g of γ-Al_2O_3 (Shanghai Xinnian Chem Co.) and 30 mL of distilled water were mixed and stirred to form homogeneous slurry A with pH = 1–2. (2) 6 g of HBeta powder (Shanghai Xinnian Chemical Co, SiO_2/Al_2O_3 = 32) was added to 20 mL of distilled water and stirred for 30 min at *r.t.* to form slurry B with pH = 8–9. (3) 8.79 g of di-iso-propylamine, slurry A and slurry B were mixed and stirred to form homogenous slurry C with pH = 8–9. Subsequently, slurry C was transferred to an autoclave (100 mL, Toflon-lined stainless steel autoclave). (4) The crystallization of slurry C was done at 200 °C for 35 h. After the crystallization was completed, the autoclave was quenched with cool water. (5) Being filtered and washed thoroughly with distilled water, the solid product was dried at 110 °C for 3 h and then calcined at 540 °C for 6 h in air flow for burning off the template.

2.1.2. The mechanical mixture

The mechanical mixture of SAPO-11/HBeta was prepared by using fully blending of HBeta (Shanghai Xinnian Chemical Co, SiO_2/Al_2O_3 = 32) and the as-synthesized SAPO-11. The sample was remarked as SB-M. SAPO-11 was typically synthesized as the following steps, (1) 11.97 g of H_3PO_4 (85 wt%, Beijing Chem. Co., A.R.), 5.58 g of γ-Al_2O_3 (Shanghai Xinnian Chem Co.), 0.20 g fumed SiO_2 powder and 30 mL of distilled water were mixed and stirred to form homogeneous slurry D with pH = 1–2. (2) 8.79 g of di-isopropylamine was added to the slurry D and then stirred to form homogenous slurry E with pH = 8–9. (3) The crystallization of slurry E was done at 200 °C for 35 h in an autoclave (100 mL, Toflon-lined stainless steel autoclave). After the crystallization was completed, the autoclave was quenched with cool water. Being filtered and washed thoroughly with distilled water, the solid product was dried at 110 °C for 3 h and then calcined at 540 °C for 6 h in air flow for burning off the template.

The weight fraction of SAPO-11 in the samples was estimated from a plot of XRD peak intensity vs. weight fraction of SAPO-11. The plot could be obtained by correlating the relationship of XRD peak intensity of SAPO-11 (2θ = 23.3°) with the known SAPO-11 weight fraction in SAPO-11/Beta mixture prepared by mechanical blending method.

2.2. Characterization

The materials were respectively characterized by using N_2 isothermal adsorption-desorption, XRD, IR, ^{27}Al MAS NMR, ^{31}P MAS NMR and Py-IR.

N_2 isothermal adsorption–desorption characterization of the samples was performed at the temperature of liquid nitrogen by using Micromeritics ASAP400 adsorptionmeter. The sample (ca. 240 mg) was degassed at 200 °C and 10^{-6} mmHg before the measurement of data. The specific surface area (S_{BET}) was calculated according to BET method and the volume of porous (V_{pore}) was obtained by *t*-plot analysis of the adsorption isotherm.

Powder X-ray diffraction (XRD) patterns were collected by Rogaku Rotflex D/Max-C powder X-ray diffractometer with CuKα radiation (λ = 0.15046 nm) operated at 40 kV and 30 mA to identify the phase structure of the catalysts.

IR spectra were recorded with using a Bruker IFS113V FTIR spectrometer. The IR spectrometer was equipped with an *in situ* cell containing CaF_2 windows. About 11.5 mg sample was pressed into self-supported disc, which was introduced into the cell. The disc was firstly heated to 400 °C for 2 h in air flow. Secondly, it was cooled down to room temperature under vacuum in He flow and IR spectra of samples were recorded.

In Py-IR experiments, the sample disc was activated under vacuum and He flow at 400 °C for 2 h and then cooled down to 150 °C. Subsequently, He flow saturated with pyridine was introduced into the IR cell at 150 °C for 2 h to ensure that all acid sites were covered. Before measuring the spectra, the samples were purged by He flow and evacuation at 150 °C for 2 h to remove physically adsorbed pyridine (IR bands at 1590 cm^{-1} completely disappeared). The Py-IR spectra were recorded at specific temperature. IR bands were measured with respect to two T–O–T stretching vibration of framework (1870 and 1981 cm^{-1}). The area of IR band at 1981 cm^{-1} was used as internal standard for the quantitative measurement.

^{27}Al MAS NMR and ^{31}P MAS NMR spectra were recorded on a Varian Unity INOVA-300 spectrometer with the frequency of 78.15 and 121.41 MHz, respectively. The probe was multinuclear 7 mm CP/MAS probehead. Forty-five-degree pulses were used for all measurement with repetition time 3 s. Data was obtained at a MAS speed of 7 kHz. Aluminum nitratein water and 85 wt% phosphoric acid were employed as references for chemical shift. All samples were equbilirated at the ambient humidity before packing into the rotors.

2.3. Catalytic test

The catalytic performance of the samples in 2-butylene cracking reaction was tested in a continuous down-flow fixed-bed reactor, which was 400 mm long and 10 mm *id.* stainless steel line. The catalyst loading in each run was ca. 1 g (20–40 mesh). The space up and down the catalyst bed in the reactor was filled with quartz chips. The reaction temperature was controlled and measured by using temperature-controller and thermal couple. Before each test, the catalyst was firstly gradually heated to the specific reaction temperature in 20 mL/min N_2 flow, and then feed was injected into the catalyst bed by a syringe pump. The product was quenched by ice bath and separated to gas and liquid products. The feed and gas-phase products were analyzed with a gas chromatograph (Hewlett-Packard model 5890-II, FID, N_2 carrier) equipped with Al_2O_3 columns for the separation of methane, ethane, ethylene, propane, propylene, *n*-butane, iso-butane, 1-butene, 2-butene and iso-butene, etc. The liquid products and C_4 olefins were analyzed by a gas chromatograph (Hewlett-Packard model 5890-II, FID, N_2 carrier) equipped with PONA columns. The feed composed of 3.6% wt of butane and 96.4% wt 2-butylene. Mass balance greater than 95% wt was used. Conversion, selectivity and yield were respectively defined as following:

2-butylene coversion wt% = $100 \times (\text{2-butylene}_{\text{converted}}/\text{2-butylene}_{\text{feed}})$

Product selectivity wt% = $100 \times (\text{product}/\text{2-butylene}_{\text{converted}})$

Product yield wt% = $100 \times$ 2-butylene conversion $\times$ product slectivity

3. Results and discussions

3.1. Characterization

3.1.1. XRD and N_2 isothermal adsorption–desorption characterization

XRD patterns of SB-H and SB-M samples are shown in figure 1. In addition, XRD patterns of SAPO-11 and HBeta are given as references. SB-M sample showed all characteristic XRD peaks of SAPO-11 and HBeta at the same $2\theta^{o}$. Although the corresponding XRD patterns of SB-H sample slightly shifted toward to lower $2\theta^{o}$ comparing with those of SAPO-11 and HBeta, SB-H sample presented all characteristic XRD peaks of SAPO-11 and HBeta. The results indicate that SAPO-11/HBeta could be synthesized by hydrothermal method, and there was slight lattice distortion of TO_4 unit in SB-H sample. On the other hand, SB-H sample showed lower S_{BET} and V_{pore} than SB-M sample despite they had similar SAPO-11 content (table 1).

3.1.2. IR characterization

Figure 2 shows IR spectra of HBeta, SAPO-11, SB-H and SB-M. IR bands in the range of 400–1300 cm^{-1} were due to the vibration of framework of molecular sieve [11–13]. According to the previous references [11–13], possible assignment of the observed IR bands was summarized in table 2.

It can be seen in figure 2, SB-H and SB-M samples showed all characteristic IR bands which could be respectively attributed to HBeta and SAPO-11. It is worth noticing, IR bands belonging to v_{asym} and v_{sym} of TO_4 on SB-H sample shifted toward lower wavenumber comparing the corresponding IR bands detected on SB-M, SAPO-11 and Beta. The results imply that SAPO-11 and Beta chemically bonded and presented slight lattice distortion of TO_4 unit in SB-H sample. The results is agreement with the results of XRD.

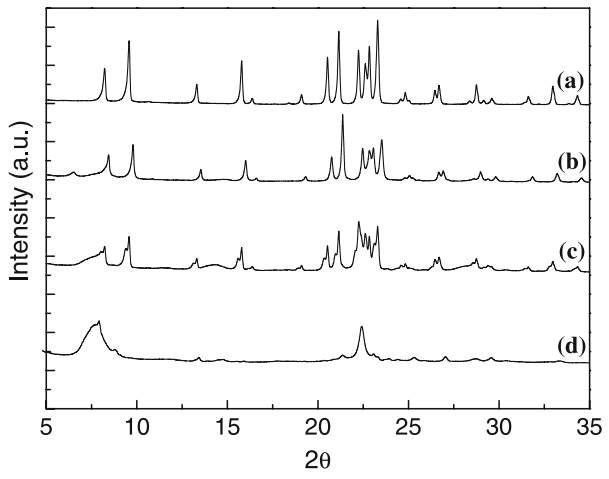

Figure 1. XRD patterns of (a) SAPO-11, (b) SB-M, (c) SB-H and (d) HBeta.

Table 1
SAPO-11 content, S_{BET} and V_{pore} of the samples

Sample	SAPO-11 (%wt)	S_{BET} (m^2/g)	V_{pore} (cm^3/g)
SB-H	0.55	229	0.10
SB-M	0.55	244	0.13

On the other hand, new IR bands at 895 and 942 cm^{-1} were observed on SB-H sample, which could be attributed to v_{asym} of new species containing with TO_4 [11–13]. These results suggest that new species containing TO_4 formed during the hydrothermal synthesis processes of SB-H sample.

3.1.3. ^{27}Al and ^{31}P MAS NMR characterization

^{27}Al and ^{31}P MAS NMR were used to further uncover the chemical environment of framework and non-framework elements in the samples. ^{27}Al and ^{31}P MAS NMR spectra of HBeta, SAPO-11, SB-H and SB-M samples are shown in figure 3. As can be seen, SB-M and SB-H samples showed two ^{27}Al signals at 36.1 and 52.3 ppm, which respectively originated from tetrahedral aluminum in the framework of SAPO-11 and HBeta. In addition, SB-H sample presented a new weak ^{27}Al signal at 5.6 ppm, due to the presence of a small amount of amorphous aluminum in the sample [7,8].

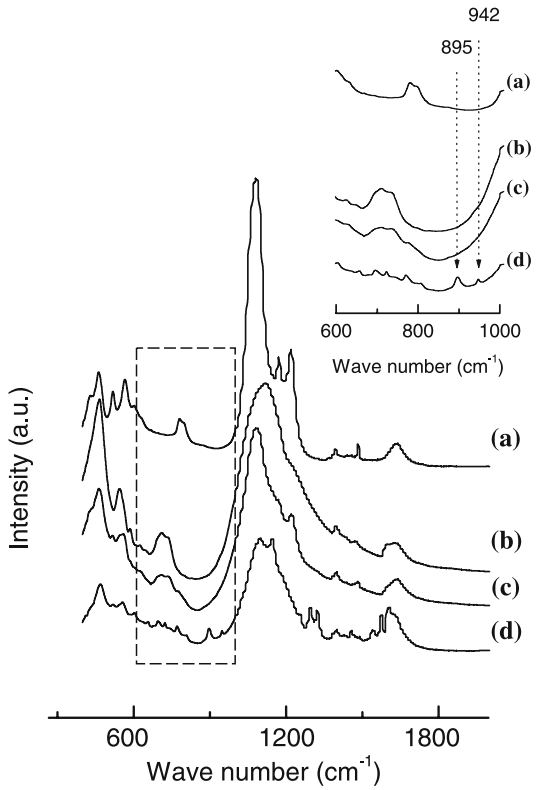

Figure 2. IR spectra of (a) HBeta, (b) SAPO-11, (c) SB-M, (d) SB-H.

Table 2
Position and possible assignments of the observed IR bands on these samples

Type	Vibration	HBeta	SAPO-11	SB-H	SB-M
Inner and external TO_4	ν_{asym}	1218 (ms)	1224 (ms)	1215 (w)	1221 (ms)
		1171 (ms)	1125 (s)	1144 (s)	1171 (ms)
		1085 (s)		1092 (s)	1085 (s)
				942 (w)	
				895 (w)	
	ν_{sym}	799 (ms)	742 (ms)	725 (w)	745 (ms)
		779 (ms)	712 (ms)	695 (w)	712 (ms)
	T–O binding and double rings	600 (ms)	593 (w)	606 (w)	
		566 (ms)	546 (ms)	559 (w)	566 (w)
		519 (ms)		519 (w)	519 (w)
		466 (ms)	466 (ms)	466 (ms)	466 (ms)

w: weak; ms: mid-strong; s: strong.

With regard to ^{31}P MAS NMR spectra, a sharp signal at ca. −30.6 ppm was detected in all investigated samples, which was attributed to tetrahedral phosphorous in the framework of SAPO-11. In the particular case of SB-H, a new ^{31}P signal at ca. −18.2 ppm was observed, tentatively due to the presence of defect $P(AlO_4)_n$ ($n < 4$) unit [9,10]. Combining with the results of XRD and IR, we deduce that the defect $P(AlO_4)_n$ ($n < 4$) unit caused the presence of new IR bands.

On the basis of the above results, we can find that the defect $P(AlO_4)_n$ ($n < 4$) unit really existed in SB-H samples. During the hydrothermal synthesis process of SB-H sample, the framework of HBeta was at least partly "solved" in the basic solution to support silica source and serviced as seed for the crystallization of SAPO-11. Under the used hydrothermal conditions, SAPO-11 and HBeta chemically bond and the defect $P(AlO_4)_n$ ($n < 4$) unit formed in SB-H sample.

3.1.4. Py-IR characterization

The acidity of SB-M and SB-H samples was respectively investigated by Py-IR. Py-IR spectra in the range from 1400 cm^{-1} to 1700 cm^{-1} were recorded and are shown in figure 4. IR bands at 1455 and 1545 cm^{-1} were observed, due to the characteristic bands of pyridine chemisorbed on L and B acid sites, respectively [15–18]. IR band appearing at 1490 cm^{-1} was attributed to pyridine co-adsorbed on both B and L acid sites [15–18]. The results demonstrate that B and L acid sites existed on SB-H and SB-M samples. When the samples were heated from 200° C to 350° C, IR bands at 1455, 1545 and 1490 cm^{-1} still could be detected, but the half-width and intensity of these bands distinctly decreased. These results indicate that there were strong acid sites on the samples, in addition, the weak and mid-strong acid sites desorbed from the samples surface as the temperature elevating.

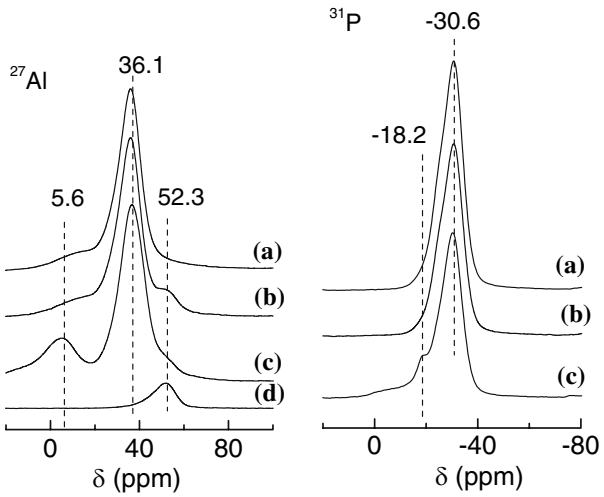

Figure 3. ^{27}Al and ^{31}P MAS NMR spectra of (a) SAPO-11, (b) SB-M, (c) SB-H and (d) Hbeta.

The amount and the distribution of acid sites were estimated and the results are summarized in table 3. It is found that SB-H sample had quite different acidic amount and acidic distribution comparing with SB-M sample. SB-H sample possessed more B acidic amount and higher B/L ratio than SB-M sample. Contrarily, SB-M sample had more L acid amount than SB-H sample.

We think that the difference on acidity between SB-H and SB-M samples can be due to the formation of the defect $P(AlO_4)_n$ ($n < 4$) unit in SB-H sample. We would like to propose the following explanation to account for the effect of defect $P(AlO_4)_n$ ($n < 4$) unit on the acidity. In the case of $P(AlO_4)_n$ ($n < 4$) unit, aluminum sites require charges to compensate protons, probably terminated by OH group, therefore, new B acidic sites produces on SB-H sample. Therefore, B acidic amount and B/L ratio were more on SB-H sample than those on SB-M sample.

3.2. Catalytic performance of 2-butylene cracking

The catalytic performance of SB-M and SB-H samples in cracking of 2-butylene was tested, respectively. The results are given in table 4. First, we made blank experiments, that is, we investigated effects of reactor inner-wall and gas-phase thermal reaction on cracking

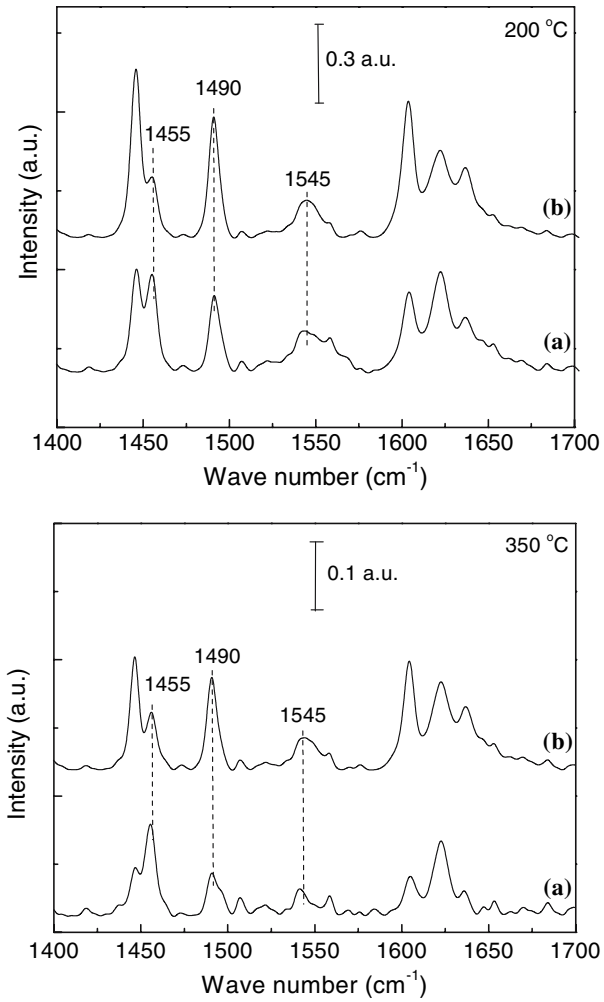

Figure 4. Py-FT-IR spectra of the samples at 200° C and 350° C, (a) SB-M and (b) SB-H.

of 2-butylene. Blank reactor gave 11.4%wt conversion of 2-butylene under the reaction conditions of 490° C, WHSV = 1 h^{-1} and 0.1 MPa. When the reactor was filled with quartz chips, we found the conversion of 2-butylene greatly decreased to ca. 2%wt under the same conditions. The results suggest that the effects of the gas-phase thermal reaction and reactor inner-wall on the cracking of 2-butylene can be signficantly reduced by filled with quartz chips in the reactor. Therefore, the space up and down the catalysts bed was filled with quartz chips in catalytic test of SB-H and SB-M samples.

Table 3
Acidic amount and distribution of acid sites on the samples

Sample	Acidic amount (a.u./g)						Distribution of acid sites		
	200		350		Total				
	L	B	L	B	L	B	B_{200}/L_{200}	B_{350}/L_{350}	B_{total}/L_{total}
SB-H	52	32	38	22	90	54	0.62	0.58	0.60
SB-M	65	28	48	15	113	43	0.43	0.31	0.38

It can be seen in table 4 that SB-H sample exhibited higher selectivity and higher yield of C_2–C_3 olefins than SB-M. In order to further compare the catalytic performance of SB-H with SB-M samples, 2-butylene conversion and selectivity of C_2–C_3 olefins are normalized in (m^2/g), which were defined as 2-butylene specific conversion and specific selectivity of C_2–C_3 olefins, respectively (table 4). We can find, SB-H sample shows similar specific conversion of 2-butylene as SB-M sample whiles the former has distinctly higher specific selectivity of C_2–C_3 olefins than the latter. On the other hand, we observed that there were more coke on SB-M sample than on SB-H sample. These results indicate that SB-H sample had higher catalytic performance in cracking of 2-butylene to C_2–C_3 olefin than SB-M sample.

Figure 5 shows effects of reaction temperature on the catalytic performance of SB-H sample in cracking of 2-butylene. As can be seen, reaction temperature (470–60° C) had great influence on the reactivity of the sample. With the increase of reaction temperature, conversion of 2-butylene monotonously increased. In case of selectivity of C_2–C_3 olefins, they exhibited gradually increase tends as the reaction temperature increasing. Similarly, the yield of C_2–C_3 olefins increased with the increase of temperature. The highest yield of propylene and ethylene respectively reached ca. 33.1 wt% and ca. 11.5 wt% at the temperature range of 530–560° C. Based on the above results, we consider that SB-H sample showed good selectivity and yield of

Table 4
Catalytic performance of catalytic cracking of 2-butylene on SB-M and SB-H samples

	SB-H	SB-M
2-butylene conversion (wt. %)	68.8	76.7
Product selectivity (wt.%)		
Methane, ethane	0.4	3.2
Ethylene	6.5	2.6
Propane	1.8	3.0
Propylene	40.2	23.1
n-Butane	3.0	5.1
Iso-butane	2.5	5.6
1-Butylene	2.3	10.6
Iso-Butylene	22.5	17.8
C_5–C_{12}	20.0	28.9
Coke	0.8	2.2
Product yield (wt.%)		
Ethylene	3.1	2.0
Propylene	27.7	17.7
T Propylene + ethylene	30.8	19.7
2-butylene specific conversion (wt.%/(m^2 g^{-1}))	0.30	0.31
Propylene specific selectivity (wt.%/(m^2 g^{-1}))	0.03	0.01
Ethylene specific selectivity (wt.%/(m^2 g^{-1}))	0.18	0.09

Reaction conditions: 490 °C, 1 g h^{-1}, 0.1 Mpa.
The data were obtained when the time on stream was 240 min.

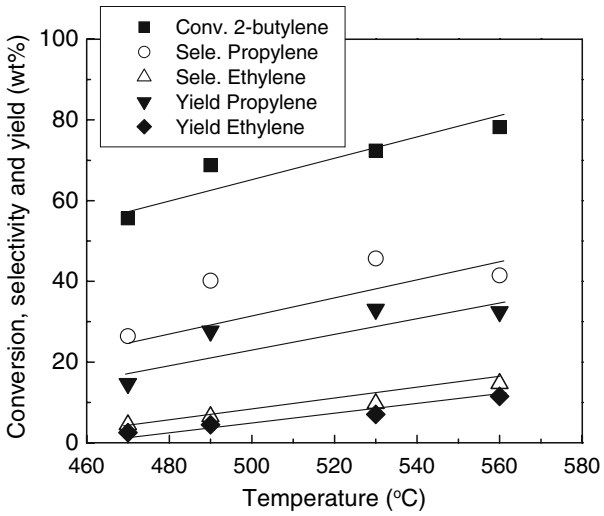

Figure 5. Effects of reaction temperature on the catalytic performance of SB-H sample in catalytic cracking of 2-butylene. The data were obtained when the time on stream was 240 min.

C_2–C_3 olefins in catalytic cracking of 2-butylene comparing with the previous catalysts.

On the other hand, we estimated apparent active energy of catalytic cracking of 2-butylene to C_2–C_3 olefins on the samples in terms of Arrhenius form of equation $v = A \times \mathrm{Exp}(-E_a/RT)$, in which v is apparent rate of produced C_2–C_3 olefins; E_a is apparent active energy, A is apparent frequency factor and T is reaction temperature (K). We hypothesized that the frequency factor A was not much changed on SB-H and on SB-M samples. The lineal plot of $\ln v$ versus $1/T$ was obtained by lineal regression method. As can be seen in figure 6, both SB-H and SB-M samples showed increasing tend of apparent rate of produced C_2–C_3 olefins with the reaction temperature increasing, as expected by thermodynamics and kinetics. E_a was obtained from slope of

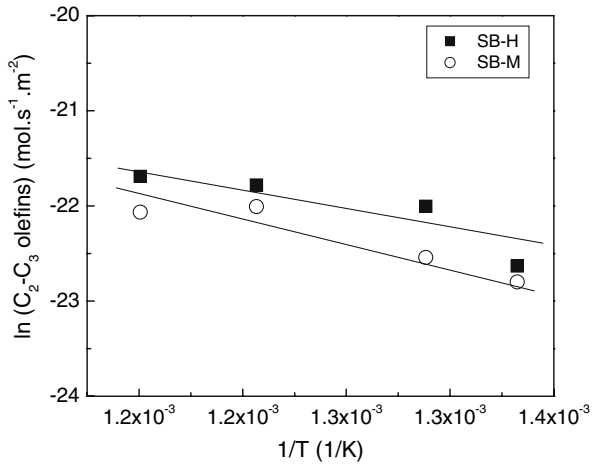

Figure 6. Arrhenius plots of SB-M and SB-H samples for catalytic cracking of 2-butylene to C_2–C_3 olefins.

the straight plot. The apparent activation energy of the reaction on SB-H sample was ca. 39.3 kJ/mol, while the apparent activation energy of the reaction on SB-M sample was ca. 55.8 kJ/mol. Therefore, the results demonstrate that SB-H sample much favored the cracking of 2-butylene to C_2–C_3 olefins comparing with SB-M sample.

SB-H and SB-M samples exhibited different selectivity and yield of C_2–C_3 olefins in cracking of 2-butylene, possibly due to the difference on acidity of SB-H and SB-M samples. The acidity of the samples was close relative to their catalytic performance in cracking of olefins [21,22]. It is generally accepted that B acid sites are active sites for the catalytic cracking of olefins to C_2–C_3 olefins [21,22]. The proper increase of B acidic amount and B acidic strength could enhance the production of C_2–C_3 olefins in the reaction [21,22]. Wang *et al.* [3] found that ZSM-23 (SiO_2/Al_2O_3 = 30) showed the maximal yield of C_2–C_3 olefins among the investigated samples during catalytic cracking of butylene, due to one of possible reasons that ZSM-23 (SiO_2/Al_2O_3 = 30) had the higher B acidity than the other catalysts. Zhu *et al.* [4,5] observed that the higher selectivity of C_2–C_3 olefins could be obtained on ZSM-5 zeolite catalyst with higher B acidity. Zhao *et al.* [6] found that ZSM-48 exhibited more excellent selectivity to propylene than ZSM-5 during catalytic cracking of C_4 olefins. They considered that the difference of catalytic performance of ZSM-48 and ZSM-5 can be attributed to the difference in acidity. In the case of this work, SB-H sample had higher B acidic amount and higher B/L ratio than SB-M, therefore, the apparent active energy of catalytic cracking of 2-butylene to C_2–C_3 olefins on SB-H sample was lower than that on SB-M sample, which resulted in the higher selectivity and higher yield of C_2–C_3 olefins on SB-H in the reaction.

On the other hand, SB-M sample had higher L acidic amount than SB-H sample. It is well known that the high L acid amount is easily to induce the formation of coke on the catalysts [21,22]. Hence, SB-M sample showed more coke than SB-H sample.

4. Conclusions

SAPO-11/HBeta composite can be synthesized by hydrothermal method. During the hydrothermal synthesis process of SAPO-11/HBeta composite, the framework of HBeta was at least partly "solved" in the basic solution to support silica source and serviced as seed for the crystallization of SAPO-11 under the used hydrothermal conditions. Therefore, SAPO-11 and HBeta chemically bonded and the defect $P(AlO_4)_n$ ($n < 4$) unit formed in SB-H sample. $P(AlO_4)_n$ ($n < 4$) unit induced new B acidic sites, therefore, B acidic amount and B acidic distribution were more on SB-H

sample than those on SB-M sample. The improvement of B acidity reduced apparent active energy of catalytic cracking of 2-butylene to C_2–C_3 olefins on SB-H sample. Therefore, the comparatively higher selectivity and higher yield of C_2–C_3 olefin were gained on SB-H sample in catalytic cracking of 2-butylene. SB-H sample is a promising catalyst for catalytic cracking of 2-butylene to C_2–C_3 olefins.

References

[1] X. Zhang, J. Wang and J. Zhong, Petrochem. Tech. 33(8) (2004) 781.
[2] Y. Lu, M. He, X. Shu and B. Zong, Appl. Catal. A 255 (2003) 345.
[3] B. Wang, Q. Gao, J. Gao, D. Ji, Wang and J. Suo, Appl. Catal. A 274 (2004) 167.
[4] X. Zhu, S. Liu, Y. Song and L. Xu, Appl. Catal. A 288 (2005) 134.
[5] X. Zhu, S. Liu, Y. Song, S. Xie and L. Xu, Appl. Catal. A 290 (2005) 191.
[6] G. Zhao, J. Teng, Y. Zhang, Z. Xie, Y. Yue, Q. Chen and Y. Tang, Appl. Catal. A 299 (2005) 167.
[7] A.M. Prakash, C.V.V. Satyanarayana, R.P. Bagwe, S. Ashtekar and D.K. Chakrabarty, Micro. Mater. 6 (1996) 89.
[8] M. Briend, A. Lamy, M.J. Peltre, P.P. Man and D. Barthomeuf, Zeolites 13 (1993) 201.
[9] C.S. Blackwell and R.L. Patton, J. Phys. Chem. 88(25) (1984) 6135.
[10] Z. Zhang and B. Zong, Chin. J. Catal. 24(11) (2003) 856.
[11] R. Xu and W. Pang, *Chemistry of Molecular Sieve and Multiporous Materials* (*Fen Zi Shai yu Duo Kong Cai Liao Hua Xue*) (Ke Xue Chua Ban She, Beijing, 2004), p. 171.
[12] E.M. Flanigen, H. Khatami, and A.H. Seymenski, *Adv. Chemistry Series,* Vol. 101, eds. E.M. Flanigen and L.B. Sand (American Chemical Society, Washington, DC, 1971), p. 201.
[13] E. Geidel, H. Bohlig and C. Peuker, Stud. Surf. Sci. Catal. 65 (1991) 511.
[14] D.M. Roberge, H. Hausmann and W.F. Holderich, Phys. Chem. Chem. Phys. 4 (2002) 3128.
[15] T.R. Hughes and H.M. White, J Phys Chem. 71 (1967) 2192.
[16] P.E. Eberly, J Phys Chem. 72 (1968) 1042.
[17] J.C. Vedrine, A. Aurox and V. Bolis, J Catal. 59 (1979) 248.
[18] N.Y. Topsøe, K. Pdersen and E. Derouane, J Catal. 70 (1981) 41.
[19] H. Liu, X. Bao, W. Wei and G. Shi, Micro. Meso. Mater. 66 (2003) 117.
[20] W. Guo, L. Huang, P. Deng, Z. Xue and Q. Li, Micro. Meso. Mater. 44/45 (2001) 427.
[21] Y.V. Kissin, Catal. Rev. 43(1&2) (2001) 85.
[22] K. Tanabe, M. Misono, Y. Ono and H. Hattori, *New Solid Acids and Bases their Catalytic Properties* (Kodausha, Tokyo, 1989).